Relativity or Aromaticity? A First-Principles Perspective of Chemical Shifts in Osmabenzene and Osmapentalene Derivatives

Cina Foroutan-Nejad[a,b*], Jan Vícha[c*], and Abhik Ghosh[d*]

a. Department of Chemistry, Faculty of Science, Masaryk University, 625 00, Brno, Czech Republic: canyslopus@yahoo.co.uk

b. National Centre for Biomolecular Research, Faculty of Science, Masaryk University, 625 00 Brno, Czech Republic

c. Center of Polymer Systems, University Institute, Tomas Bata University in Zlín, Třída T. Bati, 5678, CZ-76001, Zlín, Czech Republic: jvicha@utb.cz

d. Department of Chemistry, UiT – The Arctic University of Norway, 9037 Tromsø, Norway; E-mail: abhik.ghosh@uit.no

Abstract

We have studied the magnetic response properties and aromaticity of osmium metallacycles by means of scalar-relativistic (1c), and fully relativistic (4c) density functional theory computations. For osmabenzene, whose aromatic character has remained controversial, a topological analysis of the current density has revealed the presence of a unique σ-type Craig-Möbius magnetic aromaticity. We show that partially filled osmium valence shell is inducing large paratropic current, which may interfere with some of the methods used to study aromaticity, such as NICS. Further, we show that extreme deshielding of the light atoms in the vicinity of the osmium centers in osmapentalene derivatives is not a result of aromaticity but can be explained by paramagnetic couplings between $\sigma_{Os—C}$ bonding orbitals and the π^*_{Os} orbitals. We demonstrate that the alternating orientation of induced magnetic currents through the molecule correlates with the alternating sign of the spin-orbit contribution to the magnetic shielding.

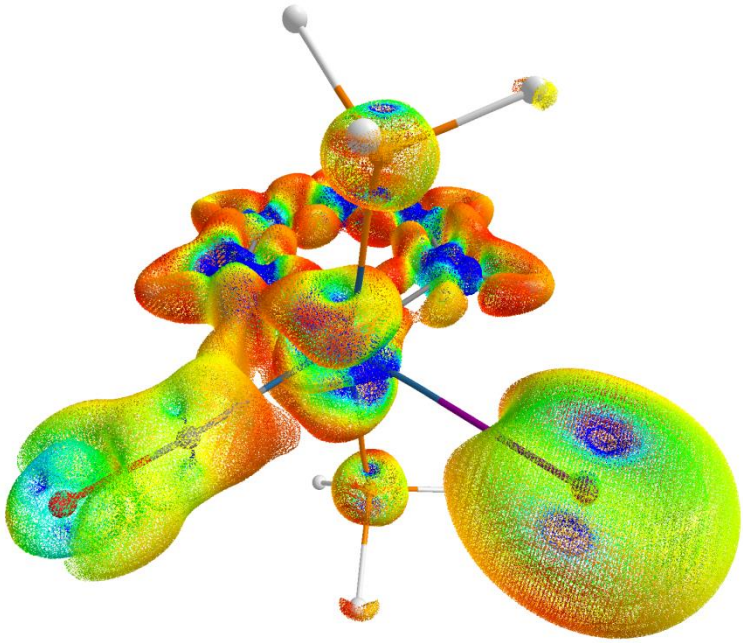

Introduction

Since Thorn and Hoffmann's proposal[1] that metallacycles may manifest aromatic character and their experimental realization by Roper and coworkers[2], the field has grown by leaps and bounds.[3–7] Thus, certain metallabenzenes have indeed been found to exhibit aromatic character and to participate in a number of classic electrophilic aromatic substitutions. Somewhat surprisingly, the aromaticity of these systems has not been analyzed in depth by means of state-of-the-art quantum chemical methods. It is well-known that heavy atoms with half-filled *d*-shells sustain strong paramagnetic currents around their nuclei.[8–11] Key theoretical approaches that have been used such as nucleus independent chemical shift (NICS)[12] and anisotropy of induced current density (AICD)[13] plots have been criticized as being questionable in certain cases.[14–19] NICS in particular cannot distinguish local paramagnetic effect of heavy elements, which influence magnetic properties of their neighboring atoms and NICS, from genuine ring current associated with aromaticity.[16,17] Therefore, to assess aromaticity of metallacycles containing metals with half-filled shells, one must look beyond NICS. Beside NICS and AICD, high-frequency ^{1}H chemical shifts of osmacycles have also been employed to as an experimental evidence in favor of aromaticity of these species. Moreover, heavy atom effect on light atoms as a result of relativistic effects (HALA effect) might be as important as aromaticity particularly for nearby ^{1}H NMR chemical shifts, but this issue has not been scrutinized in details.

Here we present a first major study of magnetically induced ring currents in a number of faithful analogues of experimentally known osmabenzene and osmapentalene derivatives, first at the scalar-relativistic level approximated by an osmium effective core potential level and subsequently at state-of-the-art all-electron four-component relativistic level. Based on the topology of the current density, we identify a special type of σ-type Craig-Möbius aromaticity for

osmabenzene and analyze the paramagnetic and relativistic contributions to the chemical shifts of neighboring light atoms and propagation of spin-orbit shielding through the molecule.

Methods

All structures were optimized and were confirmed as local minima from the second derivatives of the Hessian matrix at DFT(PBE0[20–23])/def2-QZVP,[24] computational level as implemented in Gaussian 09 rev. D1[25] suite of programs. Current densities at scalar-relativistic level (ECP approximation) were obtained from the wavefunction of GIAO NMR computations for a magnetic field applied perpendicular to the ring plane of the molecules within the context of the Quantum Theory of Atoms in Molecules (QTAIM[26–30]) using AIMAll.[31] Magnetically induced current intensities (MICs) were computed by integration of the current density passing through the zero-flux interatomic surfaces (IAS). For molecule **6**, the QTAIM-based approach failed because the Se and Os atoms do not share a common interatomic surface because of the absence of (3,-1) CP between Se and Os, **Figure 1**.[32] The current density passing through this IAS cannot be computed because the surface covers the regions that the Se is connected to both the C and Os atoms. Thus, the net current passing via this surface is zero.

Fully relativistic NMR chemical shifts were obtained at PBE0/Dyall's valence triple-zeta[33–35] level using four-component relativistic Dirac–Kohn-Sham (DKS) formalism based on the Dirac-Coulomb Hamiltonian and the restricted magnetically balanced basis for the small component,[36,37] as implemented in ReSpect 5.0 code[38] (4c level). Spin-orbit contributions to the NMR chemical shifts were obtained as the difference between the 4c and the scalar relativistic calculation with the same setup.

The MIC at the all-electron 4c and 1c levels was determined by numerical integration of the currents passing through a rectangular grid perpendicular to the plane of the ring, with one edge at the center of the ring and cutting through the center of the investigated bond. The planes were extended 6 Å beyond the bond centers and 4 Å above/below the ring planes.

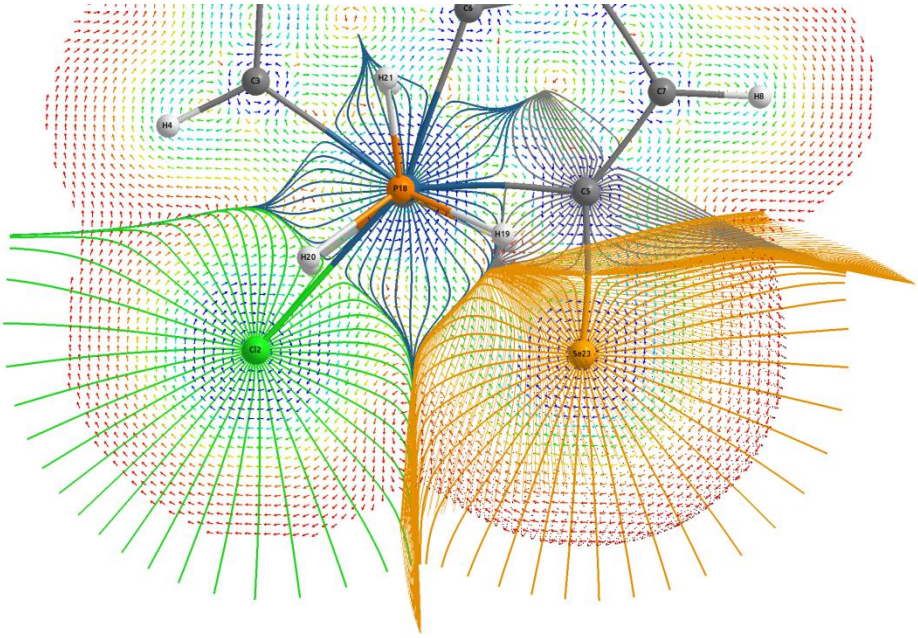

Figure 1. Representation of the atomic basins and the interatomic surface between Se and its neighboring C atom.

Results and Discussion

Current Density Analysis and Aromaticity

Chart 1 depicts the molecules studied here; by and large, they have also been examined by other authors (*vide infra*), albeit not with methods comparable to those employed here. The compounds are all formally Os(IV) with doubly occupied $5d_{xz}$ and $5d_{yz}$-based MOs. Osmabenzene

1 is the most studied molecule in this series; its aromaticity has been a controversial issue so far. The species has been described as a 6π-e Hückel aromatic system[14,39,40], 8π-e Möbius aromatic system,[6] as well as10π-e Hückel aromatic system,[41,42] but a qualitative current density analysis at B3LYP/6-31+G(d) level (with a LANL2DZ basis set or Os atoms), along with orbital-based NICS calculations suggest that osmabenzene has antiaromatic character with paramagnetic π-ring current.[15] On the other hand, the osmapentalenes **2**–**5** have been considered to be π-aromatic (**2**–**3**: 8π-e Craig-type Möbius aromatic, 5: 12π-*e* Craig-type Möbius aromatic),[43–45] while **6** has been described as a σ-aromatic selenirene ring,[46] based on their molecular orbital topologies, isomerization energies, and NICS computations.

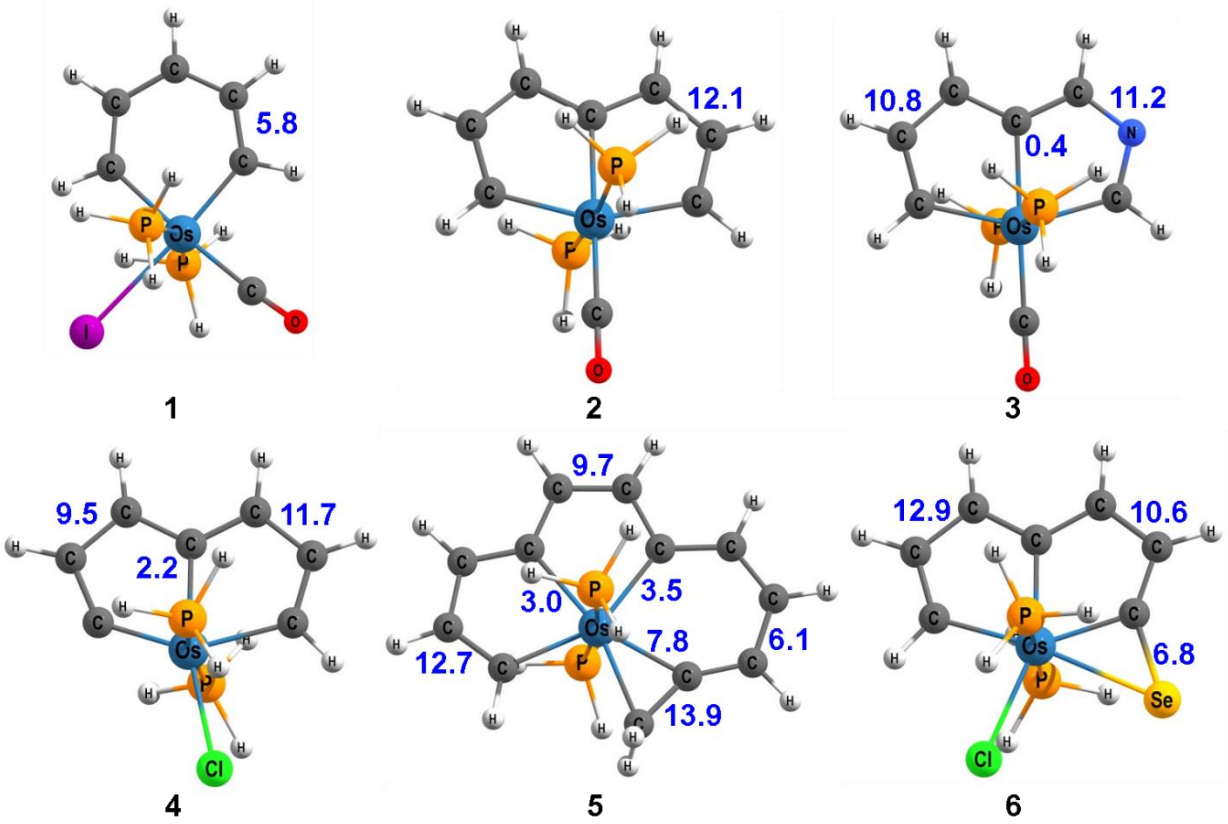

Chart 1. The structures of molecules **1**-**6** and the magnetically induced currents intensities passing through each bond in nA.T^{-1} (in blue font); the currents are computed at scalar-relativistic level, approximated by quadruple-ζ ECPs, except those for molecule **6** that are obtained from 4c computations from DFT computations by an all-electron triple-ζ basis set.

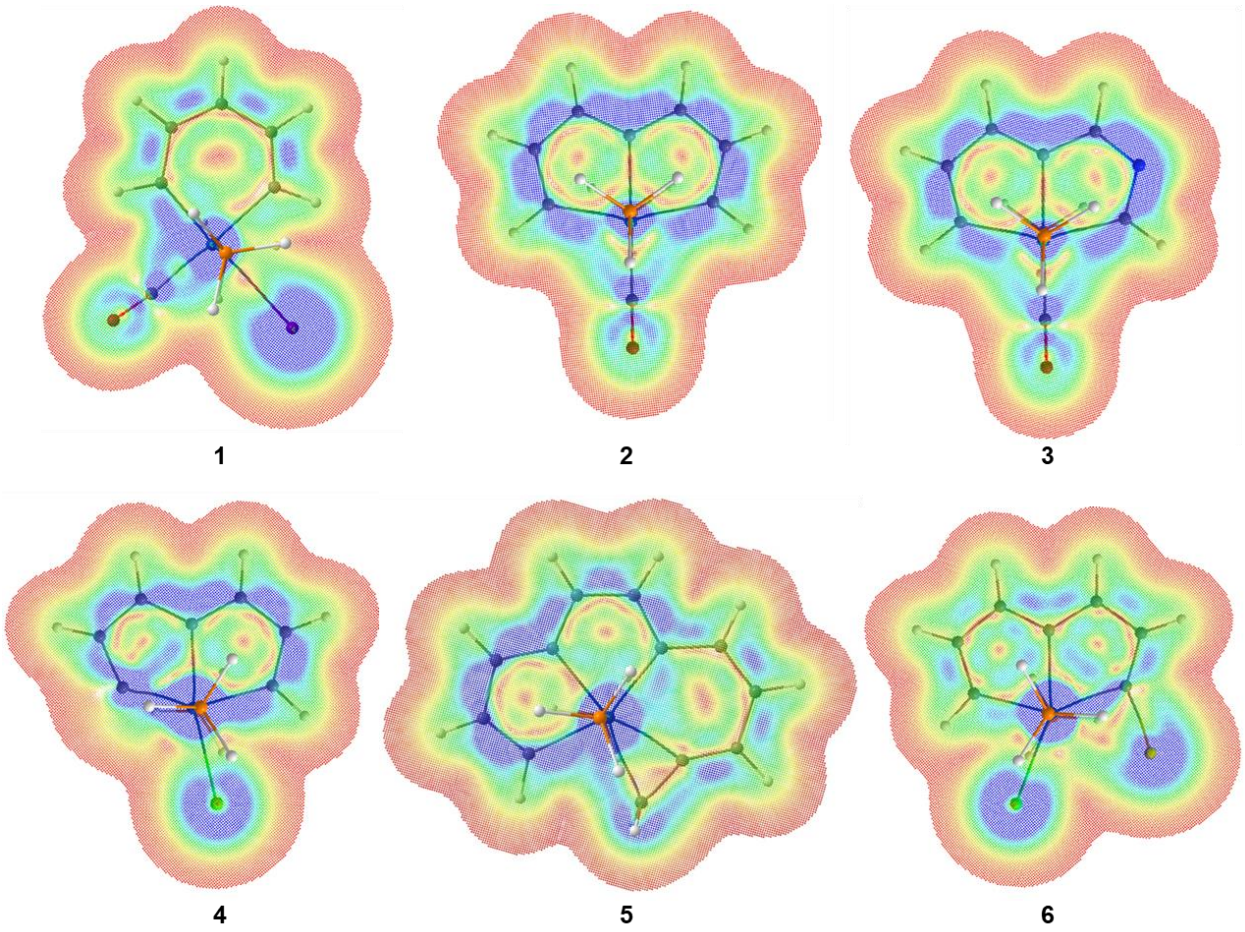

Figure 2. Current intensity plotted one atomic unit above the mean planes of the molecules studied. Red to blue colors represent 0 to 0.0005 atomic unit current density. Os atoms are recognizable with vast blue marks around them that denote strong local paramagnetic currents. PH_3 ligands are recognizable in this picture on top of the Os atoms. Please note that the Os-C bond on the right-hand-side of Os in **1** does not show characteristics of π-current, i.e. the dark blue region is missing.

Our analysis at ECP and 4c levels shows that **1** is indeed moderately magnetic aromatic and its magnetically induced current (MIC) density is about 50% of that of benzene.[47] The discrepancy between our results and those of earlier researchers may be rationalized in terms of the basis set dependence of NICS values, given that double-ζ basis sets are known to underestimate the MICs in aromatic systems.[48] **Chart 1** presents the MIC passing through selected bonds at a

scalar-relativistic level with quadruple-ζ effective core potential (ECP) basis set. In general, osmium atoms generate strong local paramagnetic currents (**Figure 2**). The local paramagnetic currents around the Os atoms stem from their half-filled 5d subshell and are known to influence magnetic shielding of neighboring atoms, a phenomenon known as the Buckingham-Stephens effect (BSE).[10,49]

To confirm scalar-relativistic results, we investigated systems **1** and **2** also using the state of the art fully relativistic (4c) calculations (**Table S1**). No significant changes in the current intensities were found when compared to 1c result. The spin-orbit coupling has only a minor contribution to the intensity of aromatic currents. This is in agreement with results of a previous study of irida- and platinabenzenes performed at two-component level.[40]

Moreover, NICS values are influenced by local paratropic current around the Os atom, because the strength of the local MIC passing between Os atom and the center of the ring calculated at 4c level are nearly –140 nA.T^{-1}, an order of magnitude larger than the aromatic ring currents in **1**. The 4c-level analysis shows that the contribution of spin-orbit (SO) coupling in local paramagnetic current around Os atom is only –5 nA.T^{-1}.

The 3D topology of the current density (**Figure 3**) suggests that **1** cannot be classified as a π-aromatic system because the current density around the osmium atom forms a pattern akin to $5d_z^2$ orbital that does not have proper symmetry to overlap with *p*-orbitals of carbon atoms. However, the central lobe of the d_z^2-shaped topology interacts with current density passing through C1 (see **Chart 2** for numbering and **Figure S1** for views from other directions and at different isosurface values of current density), but the axial lobes of d_z^2-type pattern are connected to the ring current passing through C5 of osmabenzene. The profile of the MIC 1 bohr above the ring plane (**Figure 2**) shows that the π-current is nearly absent along the Os–C1 bond; this is consistent

with previous observation by Periyasamy et. al.[15] Therefore, the current can only be of σ-type ring current accompanied with local π-currents, circulating on top of CC double bonds. The nodal planes of the d_z^2-type topology on the Os atoms separate the σ-type currents on the C1 and C5 sides of the molecule that is consistent with a Craig-type[50] Möbius aromatic system. It is worth noting that a Craig-type Möbius aromatic system is one in which the presence of a *d* atomic orbital introduces a phase-change in the wavefunction of the system. In this case, d_z^2 orbital introduces the required phase change. Such behavior is usual for pπ-dπ bonding, where $d_{xz/yz}$ orbitals are involved as recently been discussed by Szczepanil and Solà.[51] Craig-type Möbius systems may accordingly be planar with no twist observable in the overall topology of the molecule (**Figure 3.2**). The present example, however, is unique in that a d_z^2-type orbital is involved in the wavefunction's phase-change, resulting in overall σ-aromaticity (**Figures 3.1** and **S1**).

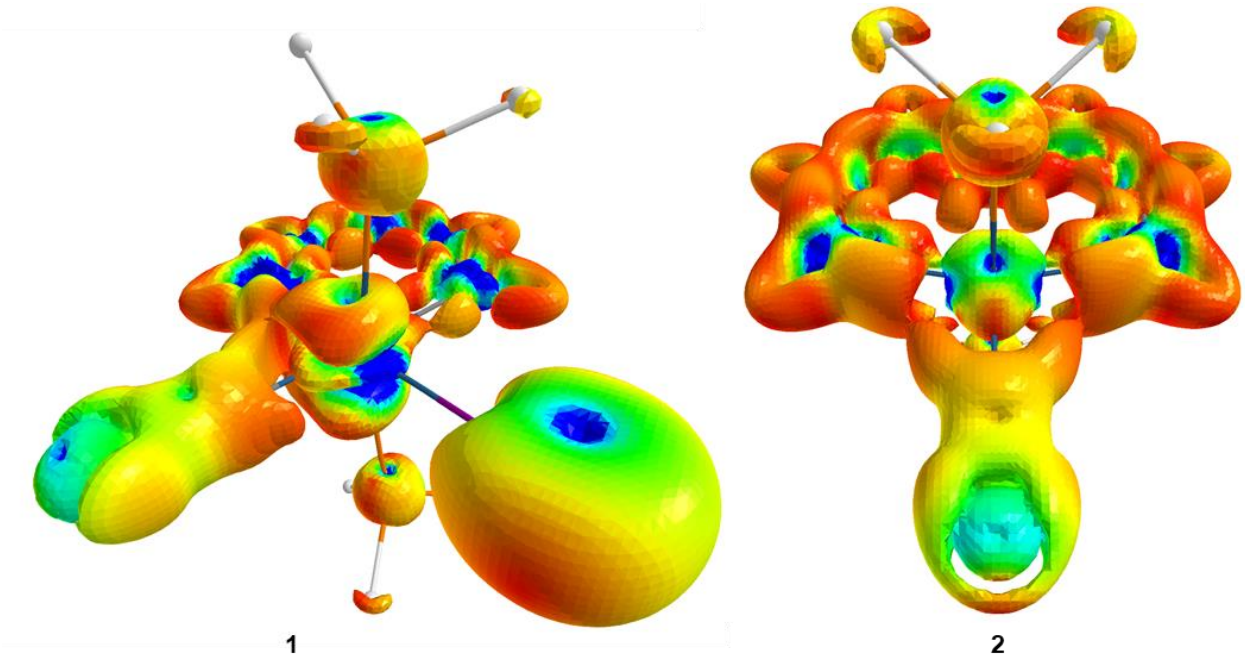

Figure 3. Isosurface of current density at j = 0.0005 au for a magnetic field applied perpendicular to the ring plane of molecules **1** and **2**. To make the nodal plane more visible, false colors have been added to the isosurface. False colors are generated by high-lighting the current intensity on j = 0.0005 au isosurface of perpendicular magnetic field for a second field that is applied along the ring plane of the molecule.

Previous analyses[52] have shown that replacing a bridging carbon in pentalene with Os(IV) changes the antiaromatic character of the molecule to aromatic. Our MIC analysis confirms this finding, since molecules **2-6** all sustain diatropic currents, between 2.2 (weak) to 13.9 nA. T^{-1} (strong), see **Chart 1**. The strength of the local paramagnetic MIC passing between Os atom and the center of rings calculated at 4c level for **2** is notably weaker than in **1**, about – 80 nA T^{-1}**,** but still significantly stronger than the aromatic ring current. Therefore, local current around Os atoms can still affect NICS values in the center of the rings far more than the ring current.

Möbius aromaticity of these systems cannot be inferred from the topology of the current density (**Figures 3** and **4**). For Craig-type aromaticity, when d_{xz} or d_{yz} atomic orbitals are involved,[51] the topology of current density is not a reliable indicator of Möbius aromaticity as the twist in the ring current topology cannot be identified because of the symmetry of $d_{xz/yz}$ orbitals. Interestingly, the topology of the current density shows that in molecules **2** and **3**, where the Os is bearing a carbon monoxide, a substantial part of the MIC passes through space via the carbon atom of the CO ligand. The Os atom remains only loosely connected to its neighboring carbons in the electronic current density (**Figures 3** and **4**). This picture is different from the usual topology of current density in hydrocarbons, where all atoms are connected to each other via the ring current.[53–56] This pattern in molecule **4** in which Os atom is connected to a chloride ligand, is absent.

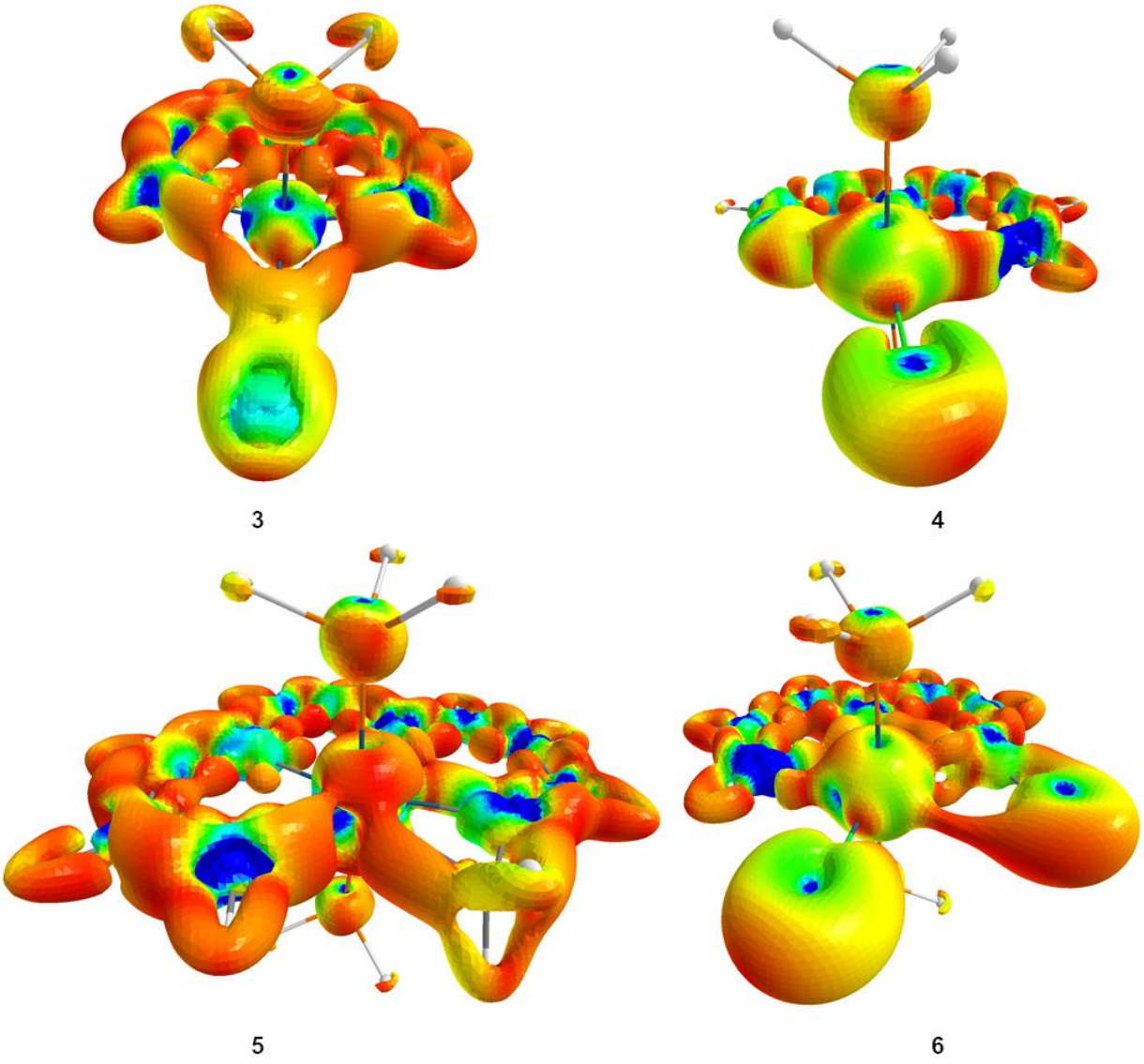

Figure 4. Isosurface of current density at J = 0.0005 au for a magnetic field applied perpendicular to the ring plane. To make the node more visible false colors are added to the figure. False colors represent the current intensity on the aforementioned isosurface for a field that is applied along the ring plane of the molecule.

Molecule **5** has been characterized as a 12c-12e pπ-dπ Craig-Möbius aromatic system and exhibits a complex ring current pattern.[45] While a strong diamagnetic current flows around the outer rim of the molecule, each ring also sustains a local current that are 3.0, 3.5, and 6.1 nA.T^{-1} for two 5-membered and 6-membered rings, respectively (**Chart 1**). The currents from all the rings

add up to 12.6 nA.T^{-1} and pass through the three-membered ring, which sustains only a weak local current (1.3 nA.T^{-1}). All local currents add up to produce 13.9 nA. T^{-1} pseudo-σ-current around the outer rim of the 3-membered ring. We refer to the current passing via the σ-bond of the cyclopropane ring as pseudo-σ because this current is in fact the molecular π-current that passes through the CH_2 group, as is usual in homoaromatic molecules; see bifurcation of the current at CH_2 (**Figure 4**).[53]

For molecule **6**, the MIC is only reported at 4c level because of anomalous topology of the electron density (see **Methods** for details). Isodesmic and NICS computations suggest that the selenirene ring in **6** is σ-aromatic [46] and that it sustains a ring current that is about 3 times stronger than that of its neighboring rings (NICS = –30.1 ppm for selenirene vs. –10.1 ppm and –8.5 ppm for 5-membered rings).[46] According to the 4c MIC, however, the current intensity of the selenirene ring is about 50% weaker than that in the 5-membered rings, being 6.8 and 12.9 nA. T^{-1} respectively, see **Chart 1**. The remarkable NICS value at the center of selenirene ring is an artifact because of the proximity of Os atom and the local paratropic current around the Os atom.[16,17]

Analysis of Magnetic Shielding

We performed NMR chemical shift analysis on two molecules (**1** and **2**) at the fully relativistic (4c) level to understand the influence of the Os atoms on the chemical shifts of adjacent light atoms (LA)[36–38] (**Table 1, S2, S3**). According to the classic Buckingham-Stephens effect (BSE) model, a strong paratropic current around the Os centers should induce diatropic currents at neighboring light atoms (LA).[10,49] However, the NMR chemical shifts of the LAs in the vicinity of the Os, δ(LA), are highly deshielded, up to 250 ppm for ^{13}C and 16 ppm for ^{1}H (**Chart 2**).[43] Indeed, the magnetic shielding tensor analysis for C1 and C5 in **1** revealed ~200 ppm of shielding in the σ_{33} tensor component perpendicular to the ring plane (z-axis), see **Figure 5** for orientation

of Cartesian system. This is a manifestation of the secondary diamagnetic MIC around the carbon atoms in the plane of the ring, induced by the paramagnetic current around the Os center (BSE effect). However, at the same time, the σ_{11} tensor component parallel with Os–C bond (x-axis) is deshielded by –350 ppm (**Table 1**), which indicate the presence of strong paratropic MIC around C1 and C5, perpendicular to the Os–C bonds.

In terms of the more intuitive orbital magnetic couplings, the –350 ppm of deshielding was found to be the result of local Ramsey-type paramagnetic coupling between bonding $\sigma_{Os—C}$ and the π^*_{Os} orbitals. A similar coupling mechanism has previously been found responsible for highly deshielded ^{13}C resonances in early-transition metal alkylidene complexes.[57] The deshielding of the LAs in the vicinity of the Os is thus not a direct result of aromaticity, as was suggested before,[43] but a product of paramagnetic coupling between bonding $\sigma_{Os—C}$ and the π^*_{Os} orbitals.

Table 1: Principal components of NMR chemical shielding tensor, **σ**, for C1, C5, H6 and H10 in compound **1** and their projection to Cartesian axes, in ppm.

	$\boldsymbol{\sigma_{11}}$	$\boldsymbol{\sigma_{22}}$	$\boldsymbol{\sigma_{33}}$	$\boldsymbol{\sigma_{xx}}$	$\boldsymbol{\sigma_{yy}}$	$\boldsymbol{\sigma_{zz}}$
C1	-382.7	-67.6	213.4	-382.7	-67.6	213.4
C5	-312.4	-53.1	188.1	-312.4	-53.1	188.1
H6	1.0	17.3	26.0	1.0	26.0	17.3
H10	4.6	17.5	32.5	32.5	4.6	17.5

In line with the recently established role of periodic trends dictating the sign of SO contribution,[8] the SO contribution to the NMR chemical shift (δ^{SO}) of vicinal carbon atoms in **1** is strongly shielding (33 ppm and 24 ppm for C1 and C5, respectively, see Table S3). The δ^{SO} is thus partly reducing the paramagnetic deshielding effect. The sign of the SO contribution also oscillates with the distance from the heavy element in both **1** and **2**, see **Chart 2-2** and **Figure 5**, following the pattern akin to J-coupling.[9] The presence of external magnetic field induces the spin-orbit

coupling in the spin density around HA, which in turn is propagated via chemical bonds by spin-polarization mechanism. This has been studied before also for aromatic systems involving heavy elements[58,59] and can be visualized using so-called "spin-orbit and magnetically induced spin density (SOM-ISD) plots".[8] The SOM-ISD plot for **1** at 4c level is given in **Figure S3**.

Propagation of spin-orbit induced magnetic shielding, σ^{SO}, is accompanied by alternating directions of the SO-MIC at given light atoms and the σ^{SO} is directly related to the strength of the SO-MIC at the light-atom nuclei.[8,11] Local SO-MIC for Os, C1, H6, C5, and H10 in molecule **1** calculated at 4c level are visualized in **Figure S2** and **Figure 5b**. As it is evident in the figures, SO coupling and induced external magnetic field form a paratropic current around the osmium atom, which induces an opposite (diatropic) SO-MIC around the C1 and C5 nuclei and again a paratropic current around H5 and H10, in agreement with the calculated alternation of the sign of σ^{SO}. Correlation between the orientation of the magnetic current and the sign of σ^{SO} is even more pronounced in symmetrical system **2** (**Figure 4c**), where contrary to **1**, the *trans* effects do not affect the magnitude of the σ^{SO}(LA) for the distant atoms.[60]

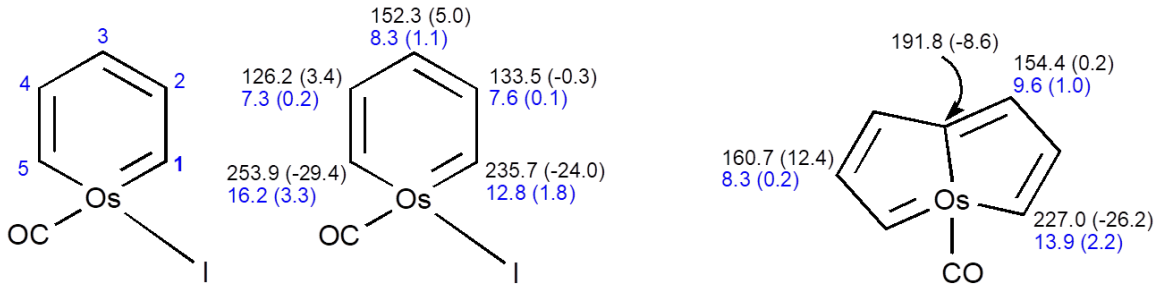

1 **2**

Chart 2. Numbering of atoms in molecule **1** and $\delta(^{13}C)$ in black and $\delta(^{1}H)$ in blue (ppm); the $\delta^{SO}(^{13}C)$ and $\delta^{SO}(^{1}H)$ values are presented in parenthesis.

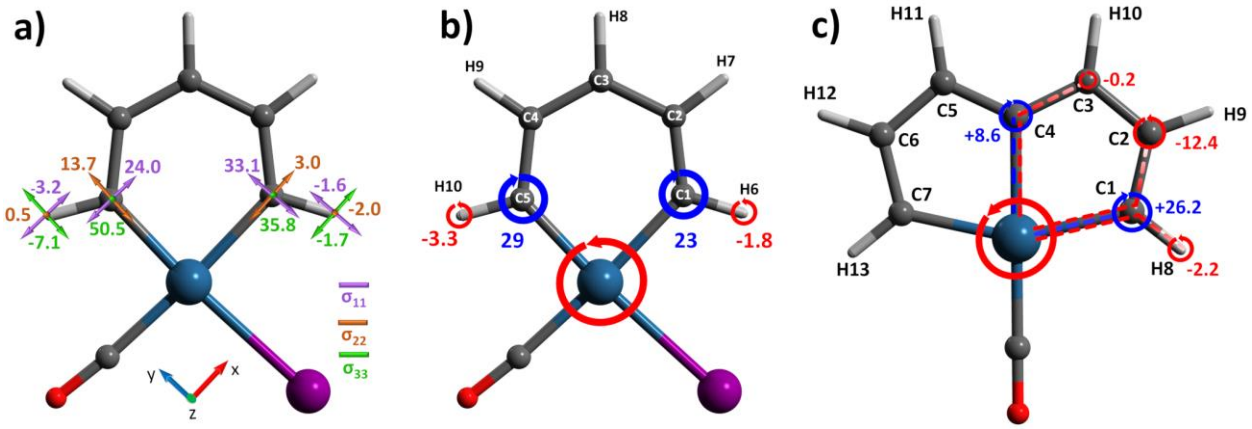

Figure 5. a) Orientation of $\boldsymbol{\sigma^{SO}}$ principal components σ^{SO}(LA) in ppm for **1**; b) schematic representation of SO-MIC around C1, C5, H6 and H10 in **1** and c) around C1-C4 and H8 in **1** together with σ^{SO}(LA) in ppm. Blue color is associated with σ^{SO}(LA) shielding (diatropic SO-MIC) while red color represents σ^{SO}(LA) deshielding (paratropic SO-MIC).

Conclusions

In conclusion, our analyses confirm a diverse spectrum of various degrees of magnetic aromaticity, from weak to as strong as benzene, of a set of archetypal osmacycles. However, the nature of the magnetic aromaticity and local effects as previously defined by MO analyses and NICS calculations are not fully confirmed by the present MIC analysis. First, osmabenzene appears best described as a σ-type Craig-Möbius aromatic system. Second, our fully-relativistic MIC analysis suggests that the very strong local paramagnetic current around the Os atoms can affect the NICS values far more than the ring current. Finally, we have shown that deshielding of light atoms in a vicinity of Os atom is not caused by aromaticity, but by local paramagnetic orbital magnetic couplings. Besides, alternation of the sign of spin-orbit contribution with increasing distance from Os reflected in alternating orientation of MIC, which makes it a valid tool for investigation of long-range spin-orbit effect.

Acknowledgements

Financial support was provided by Program I (LO1504) to J.V. Computational resources were provided under the programme "Projects of Large Research, Development, and Innovations Infrastructures" by the CESNET LM2015042, the CERIT Scientific Cloud LM2015085, and IT4Innovations National Supercomputing Center LM2015070. AG was supported by the Research Council of Norway (grant no. 262229). We thank Prof. Jeanet Conradie for MO analyses for selected systems examined herein.

Supporting information including calculated NMR chemical shifts and spin-orbit contributions and principal components of spin-orbit NMR shielding tensor at 4c-level, current density analysis for selected molecules, optimized coordinates of all studied species, and selected current density maps are available from the publisher's webpage, free of charge.

References

1 D. L. Thorn and R. Hoffmann, *Nouv. J. Chim.*, 1979, **3**, 39–45.
2 G. P. Elliott, W. R. Roper and J. M. Waters, *J. Chem. Soc. Chem. Commun.*, 1982, **0**, 811–813.
3 L. J. Wrigth, *Metallabenzenes: An Expert View*, Wiley-VCH, 2017.
4 I. Fernández, G. Frenking and G. Merino, *Chem. Soc. Rev.*, 2015, **44**, 6452–6463.
5 C. W. Landorf and M. M. Haley, *Angew. Chem. Int. Ed.*, 2006, **45**, 3914–3936.
6 J. R. Bleeke, *Chem. Rev.*, 2001, **101**, 1205–1228.
7 J. R. Bleeke, *Acc. Chem. Res.*, 1991, **24**, 271–277.
8 J. Vícha, S. Komorovsky, M. Repisky, R. Marek and M. Straka, *J. Chem. Theory Comput.*, 2018, **14**, 3025–3039.
9 M. Kaupp, O. L. Malkina, V. G. Malkin and P. Pyykkö, *Chem. – Eur. J.*, **4**, 118–126.
10 P. Hrobárik, V. Hrobáriková, F. Meier, M. Repiský, S. Komorovský and M. Kaupp, *J. Phys. Chem. A*, 2011, **115**, 5654–5659.
11 R. J. F. Berger, M. Repisky and S. Komorovsky, *Chem. Commun.*, 2015, **51**, 13961–13963.
12 Z. Chen, C. S. Wannere, C. Corminboeuf, R. Puchta and P. von R. Schleyer, *Chem. Rev.*, 2005, **105**, 3842–3888.
13 D. Geuenich, K. Hess, F. Köhler and R. Herges, *Chem. Rev.*, 2005, **105**, 3758–3772.
14 M. A. Iron, A. C. B. Lucassen, H. Cohen, M. E. van der Boom and J. M. L. Martin, *J. Am. Chem. Soc.*, 2004, **126**, 11699–11710.
15 G. Periyasamy, N. A. Burton, I. H. Hillier and J. M. H. Thomas, *J. Phys. Chem. A*, 2008, **112**, 5960–5972.

16 Z. Badri, S. Pathak, H. Fliegl, P. Rashidi-Ranjbar, R. Bast, R. Marek, C. Foroutan-Nejad and K. Ruud, *J. Chem. Theory Comput.*, 2013, **9**, 4789–4796.
17 C. Foroutan-Nejad, *Theor. Chem. Acc.*, 2015, **134**, 8.
18 C. Foroutan-Nejad, S. Shahbazian and P. Rashidi-Ranjbar, *Phys. Chem. Chem. Phys.*, 2011, **13**, 4576–4582.
19 H. Fliegl, J. Jusélius and D. Sundholm, *J. Phys. Chem. A*, 2016, **120**, 5658–5664.
20 J. P. Perdew, K. Burke and M. Ernzerhof, *Phys. Rev. Lett.*, 1996, **77**, 3865–3868.
21 J. P. Perdew, K. Burke and M. Ernzerhof, *Phys. Rev. Lett.*, 1997, **78**, 1396–1396.
22 C. Adamo and V. Barone, *J. Chem. Phys.*, 1999, **110**, 6158–6170.
23 M. Ernzerhof and G. E. Scuseria, *J. Chem. Phys.*, 1999, **110**, 5029–5036.
24 F. Weigend and R. Ahlrichs, *Phys. Chem. Chem. Phys.*, 2005, **7**, 3297–3305.
25 M. J. Frisch, G. W. Trucks, H. B. Schlegel, G. E. Scuseria, M. A. Robb, J. R. Cheeseman, G. Scalmani, V. Barone, B. Mennucci, G. A. Petersson, H. Nakatsuji, M. Caricato, X. Li, H. P. Hratchian, A. F. Izmaylov, J. Bloino, G. Zheng, J. L. Sonnenberg, M. Hada, M. Ehara, K. Toyota, R. Fukuda, J. Hasegawa, M. Ishida, T. Nakajima, Y. Honda, O. Kitao, H. Nakai, T. Vreven, J. A. Montgomery, Jr., J. E. Peralta, F. Ogliaro, M. Bearpark, J. J. Heyd, E. Brothers, K. N. Kudin, V. N. Staroverov, T. Keith, R. Kobayashi, J. Normand, K. Raghavachari, A. Rendell, J. C. Burant, S. S. Iyengar, J. Tomasi, M. Cossi, N. Rega, J. M. Millam, M. Klene, J. E. Knox, J. B. Cross, V. Bakken, C. Adamo, J. Jaramillo, R. Gomperts, R. E. Stratmann, O. Yazyev, A. J. Austin, R. Cammi, C. Pomelli, J. W. Ochterski, R. L. Martin, K. Morokuma, V. G. Zakrzewski, G. A. Voth, P. Salvador, J. J. Dannenberg, S. Dapprich, A. D. Daniels, O. Farkas, J. B. Foresman, J. V. Ortiz, J. Cioslowski, and D. J. Fox, *Gaussian 09*, Gaussian, Inc., Wallingford CT, 2013.
26 R. F. W. Bader, *Atoms in molecules: a quantum theory*, Clarendon Press, Oxford; New York, 1990.
27 T. A. Keith and R. F. W. Bader, *Chem. Phys. Lett.*, 1992, **194**, 1–8.
28 T. A. Keith and R. F. W. Bader, *Chem. Phys. Lett.*, 1993, **210**, 223–231.
29 T. A. Keith and R. F. W. Bader, *J. Chem. Phys.*, 1993, **99**, 3669–3682.
30 T. A. Keith and R. F. W. Bader, *Can. J. Chem.*, 1996, **74**, 185–200.
31 T. A. Keith, *AIMAll*, Gristmill Software, Overland Park KS, USA, 2017.
32 C. Foroutan-Nejad, S. Shahbazian and R. Marek, *Chem. – Eur. J.*, 2014, **20**, 10140–10152.
33 K. G. Dyall, *Theor. Chem. Acc.*, 2004, **112**, 403–409.
34 K. G. Dyall, *Theor. Chem. Acc.*, 2007, **117**, 483–489.
35 K. G. Dyall and A. S. P. Gomes, *Theor. Chem. Acc.*, 2009, **125**, 97.
36 S. Komorovský, M. Repiský, O. L. Malkina, V. G. Malkin, I. Malkin Ondík and M. Kaupp, *J. Chem. Phys.*, 2008, **128**, 104101.
37 S. Komorovský, M. Repiský, O. L. Malkina and V. G. Malkin, *J. Chem. Phys.*, 2010, **132**, 154101.
38 M. Repisky, S. Komorovsky, V. G. Malkin, O. L. Malkina, M. Kaupp, K. Ruud, R. Bast, M. Kadek, S. Knecht, U. Ekstrom, E. Malkin, I. Malkin-Ondik, L. Konecny and R. di Remigio, *Relativistic Spectroscopy DFT Program ReSpect, Developer Version 5.0.0*, 2018.
39 Y.-Z. Huang, S.-Y. Yang and X.-Y. Li, *J. Organomet. Chem.*, 2004, **689**, 1050–1056.
40 R. W. A. Havenith, F. D. Proft, L. W. Jenneskens and P. W. Fowler, *Phys. Chem. Chem. Phys.*, 2012, **14**, 9897–9905.
41 I. Fernández and G. Frenking, *Chem. – Eur. J.*, 2007, **13**, 5873–5884.

42 M. El-Hamdi, O. El Bakouri El Farri, P. Salvador, B. A. Abdelouahid, M. S. El Begrani, J. Poater and M. Solà, *Organometallics*, 2013, **32**, 4892–4903.
43 C. Zhu, S. Li, M. Luo, X. Zhou, Y. Niu, M. Lin, J. Zhu, Z. Cao, X. Lu, T. Wen, Z. Xie, P. v R. Schleyer and H. Xia, *Nat. Chem.*, 2013, **5**, 698–703.
44 C. Zhu, M. Luo, Q. Zhu, J. Zhu, P. v R. Schleyer, J. I.-C. Wu, X. Lu and H. Xia, *Nat. Commun.*, 2014, **5**, 3265.
45 C. Zhu, C. Yang, Y. Wang, G. Lin, Y. Yang, X. Wang, J. Zhu, X. Chen, X. Lu, G. Liu and H. Xia, *Sci. Adv.*, 2016, **2**, e1601031.
46 X. Zhou, J. Wu, Y. Hao, C. Zhu, Q. Zhuo, H. Xia and J. Zhu, *Chem. – Eur. J.*, **24**, 2389–2395.
47 T. Janda and C. Foroutan-Nejad, *ChemPhysChem*, 2018, **19**, 2357–2363.
48 Z. Badri, C. Foroutan-Nejad and P. Rashidi-Ranjbar, *Phys. Chem. Chem. Phys.*, 2012, **14**, 3471–3481.
49 A. D. Buckingham and P. J. Stephens, *J. Chem. Soc. Resumed*, 1964, **0**, 2747–2759.
50 D. P. Craig and N. L. Paddock, *Nature*, 1958, **181**, 1052–1053.
51 D. W. Szczepanik and M. Solà, *ChemistryOpen*, 2019, **8**, 219–227.
52 D. Chen, Q. Xie and J. Zhu, *Acc. Chem. Res.*, 2019, **52**, 1449–1460.
53 C. Foroutan-Nejad, S. Larsen, J. Conradie and A. Ghosh, *Sci. Rep.*, 2018, **8**, 11952.
54 A. Ghosh, S. Larsen, J. Conradie and C. Foroutan-Nejad, *Org. Biomol. Chem.*, , DOI:10.1039/C8OB01672K.
55 J. Conradie, C. Foroutan-Nejad and A. Ghosh, *Sci. Rep.*, 2019, **9**, 4852.
56 C. Foroutan-Nejad and A. Ghosh, *ACS Omega*, 2018, **3**, 15865–15869.
57 S. Halbert, C. Copéret, C. Raynaud and O. Eisenstein, *J. Am. Chem. Soc.*, 2016, **138**, 2261–2272.
58 M. Kaupp, O. L. Malkina, V. G. Malkin and P. Pyykko, *Chem.- Eur. J.*, 1998, **4**, 118–126.
59 A. Wodynski, A. Gryff-Keller and M. Pecul, *J. Chem. THEORY Comput.*, 2013, **9**, 1909–1917.
60 J. Novotný, J. Vícha, P. L. Bora, M. Repisky, M. Straka, S. Komorovsky and R. Marek, *J. Chem. Theory Comput.*, 2017, **13**, 3586–3601.